

Original Research

Modelling the Future: Groundwater Responses to Climate Change in Talomo-Lipadas Watershed, Davao City, Philippines

Nympha Ellarina-Branzuela¹

Forestry Department, College of Agriculture and Related Sciences, University of Southeastern Philippines
8100 Apokon, Tagum City, Philippines

¹Department of Forestry, CARS, University of Southeastern Philippines (USEP0), Tagum City, Philippines

† Corresponding author: Nympha E. Branzuela; nympha.branzuela@usep.edu.ph
<https://orcid.org/0000-0002-7614-2983>

| | |
|------------------------|---|
| Key Words | Climate change, Statistical downscaling method, BROOK90 hydrological model, Recharge (groundwater), Talomo-Lipadas Watersheds, Davao City |
| DOI | https://doi.org/10.46488/NEPT.2025.v24i04.D1774 (DOI will be active only after the final publication of the paper) |
| Citation for the Paper | Ellarina-Branzuela, N., 2025. Modelling the Future: Groundwater Responses to Climate Change in Talomo-Lipadas Watershed, Davao City, Philippines. <i>Nature Environment and Pollution Technology</i> , 24(4), p. D1774. https://doi.org/10.46488/NEPT.2025.v24i04.D1774 |

ABSTRACT

This research investigates the long-term impact of climate change on groundwater recharge (seepage) within the Talomo-Lipadas Watershed, Davao City Philippines, over the next eighty-nine (89) years. Employing the Statistical Downscaling Method (SDSM), station-scale climate scenarios were generated for three future time slices centered on 2020 (2011-20140), 2050 (2041-2070), and 2080 (2071-2100). These scenarios, indicating a projected increase in temperature within the watershed, were then used as input for the BROOK90 hydrological model to simulate groundwater recharge. The modelling results project a decline in groundwater supply from 109.01 million cubic meters (MCM) in 2020 to 103.53 MCM in 2050 and further down to 99.81 MCM by 2080. This projected decrease in groundwater recharge has significant implications beyond just water availability. Reduced groundwater flow can impact baseflow in rivers, affecting aquatic ecosystems and potentially exacerbating water scarcity during dry periods. Decreased recharge also has implications for other water-related sectors, including agriculture (irrigation), industry (water supply), and domestic water use, potentially leading to increased competition for dwindling resources. These findings underscore the urgent need for adaptation strategies to mitigate the effects of climate change on groundwater recharge within the Talomo-Lipadas Watershed. Further research employing diverse hydrological models is recommended to validate these findings and provide a more robust basis for developing sustainable water management plans.

INTRODUCTION

Climate change significantly disrupts watershed hydrodynamics globally, destabilizing vital water systems underpinning agriculture, ecosystem stability, and human survival. Groundwater storage, a cornerstone of freshwater sustainability (Wu et al., 2020), faces mounting threats to its availability and quality (Dao et al., 2024) due to its inherent sensitivity to the changing climate, with the manifestation of these effects intensifying in recent years (Bamala et al., 2024).

The quantifiable trends in global climate parameters demonstrate the persistence of climate change, with its consequent impacts now evident in localized environmental responses. Observational data and climate projections provide abundant evidence that freshwater resources (both surface and groundwater resources) are vulnerable and have potential to be strongly affected by climate change, with wide-ranging consequences for society and ecosystems (Bates et al., 2008). Understanding climate-change effects on groundwater is unknown and has not been explored sufficiently, because climate change may affect hydrogeological processes and groundwater resources directly and indirectly (Dettinger and Earman, 2007).

Despite growing climate change impact research, substantial knowledge gaps persist, particularly regarding localized watershed effects and the understudied groundwater resources in vulnerable regions like the Philippines. Advanced hydrological modelling is crucial for accurately assessing climate-driven groundwater storage changes, highlighting the necessity for sophisticated, region-specific research.

While recent studies (Ficklin et al., 2018; Davamani et al., 2024; Benz et al., 2024) have established climate change's disruptive influence on watersheds, demonstrating altered hydrology, ecosystem degradation, and strain on human systems, significant knowledge gaps persist. Specifically, the precise mechanisms by which climate change modifies groundwater recharge, discharge, and temperature, and the subsequent cascading effects on hydrological processes and water quality, require further investigation. For instance, while Benz et al. (2024) project a 2.1% groundwater temperature increase under a medium emissions scenario, the regional variability and long-term consequences of this warming on specific aquifer systems remain under-explored.

More scientists used models in studies of predicting hydrologic implication on climate change impacts (Flatto and Boer, 2001; Combalicer et al., 2011; P. Nyeko-Ogirambo, 2010; Zachary Pirtle et al., 2010). Of

particular interest among climate change researchers and ground water specialists is the use of Statistical Downscaling Method (SDSM) in determining the station-scale climate scenario and BROOK90 hydrological modelling (Federer, 2003) in determining the groundwater (recharge) availability of a particular watershed area. The SDSM model can produce localized, station-scale climate data from broader GCM output and generate daily weather sequences, although it does not incorporate leap years in its calculations (Combalicer et al., 2010).

BROOK90 excels in localized studies requiring detailed analysis of soil water dynamics and evapotranspiration (Federer, 2003), as demonstrated by Vorobevskii (2020) in estimating vertical water fluxes within small-scale (under 100 km²) soil-water-plant systems, while also offering an automated framework for broader water balance simulations. This detailed representation contrasts with other hydrological models like SWAT (Kiniry, 2012), which employ simplified groundwater representations and have limitations in simulating lateral flow.

For this study, A2 scenario or ‘business as usual’ was chosen to represent a high-end, but plausible, future emissions trajectory. It assumed a heterogeneous world with regionally oriented economic development, continuously growing global population, and slower technological change. It was used to explore the potential consequences of a future where emissions were not significantly mitigated. Considering, the site-specific area of the Philippines which is more likely to be compared this scenario rather than RCP scenario.

Davao City, Philippines constitutes eight subwatersheds. The Davao River Basin has an estimated drainage area or more or less 1,700 square kilometers, with an estimated length of 138 kilometers. Out of eight subwatersheds, the Talomo- Lipadas Watersheds have been prioritized for management where it supplies 99% urban population of drinking water (Hearne, 2011). By 2025, Davao City's water supply is projected to be 45% below demand compared to 1995 levels, according to the Philippines Environment Monitor (2003). This significant deficit is linked to a decrease in projected groundwater availability to 84 million cubic meters per year from 153 million cubic meters per year in 1995. The National Water Regulatory Board (NWRB) has also identified Davao City as a water-critical area.

Despite growing attention to the broad impacts of climate change, our understanding of its specific, localized effects on watersheds and groundwater resources remains critically limited, particularly within vulnerable nations such as the Philippines, and even more so in specific regions

like Davao City. Accurately assessing climate-driven changes in groundwater storage necessitates the application of advanced hydrological modelling and underscores the urgent need for in-depth, region-specific research to address this significant knowledge deficit.

2. MATERIALS AND METHODS

The study employed two open-source software namely, the Statistical Downscaling Method (SDSM) and BROOK90 hydrological modelling. SDSM simulates the eighty0nine (89) years station-scale climate projections using the work of Branzuela (2015).

Groundwater availability was simulated using the BROOK90 hydrological model. This study prioritizes the Talomo and Lipadas sub-watershed (shown in Figure 1) due to their vital role in supplying water to Davao City. These sub-watershed are the primary recharge areas for the city's groundwater, with Lipadas being the core site for the Davao City Water District's production wells. Their combined 38,374-hectare area spans the Baguio, Calinan, Toril, Talomo, and Tugbok districts.

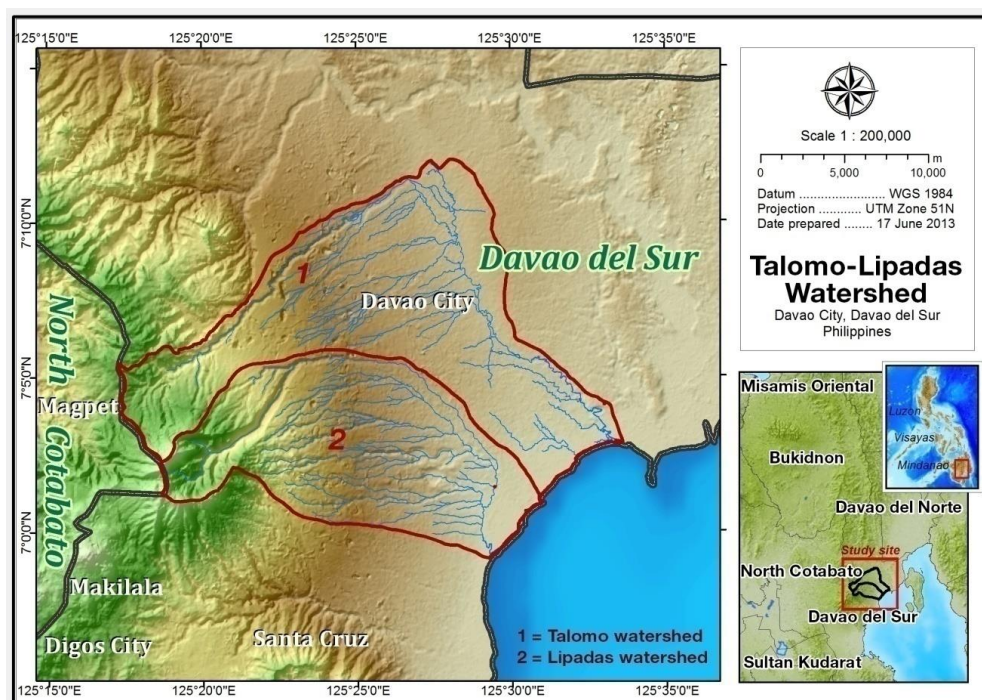


Figure 1. Location of the Study

2.1 Statistical Downscaling Method

Local information was sourced out from the Agrometeorological Station for the predictand, while larger-scale data sets from the National Centre for Environmental Prediction (NCEP) served as predictors- these models were subsequently utilized with GCM-derived predictors to generate daily weather data for a future timeframe (Wilby, 2002).

The SDSM serves as decision support instrument for evaluating the effects of climate change at the local level by utilizing a robust statistical downscaling method. SDSM enables users to identify significant large-scale climate variables (the predictors) that account for the majority of variability in the climate (the predictand) at a particular site, specifically within the two sub-watersheds, and statistical models are subsequently developed based on this data. Again, this process can be accessed in the previous publication of Branzuela et al., 2015. Figure 2 describes the generation processes.

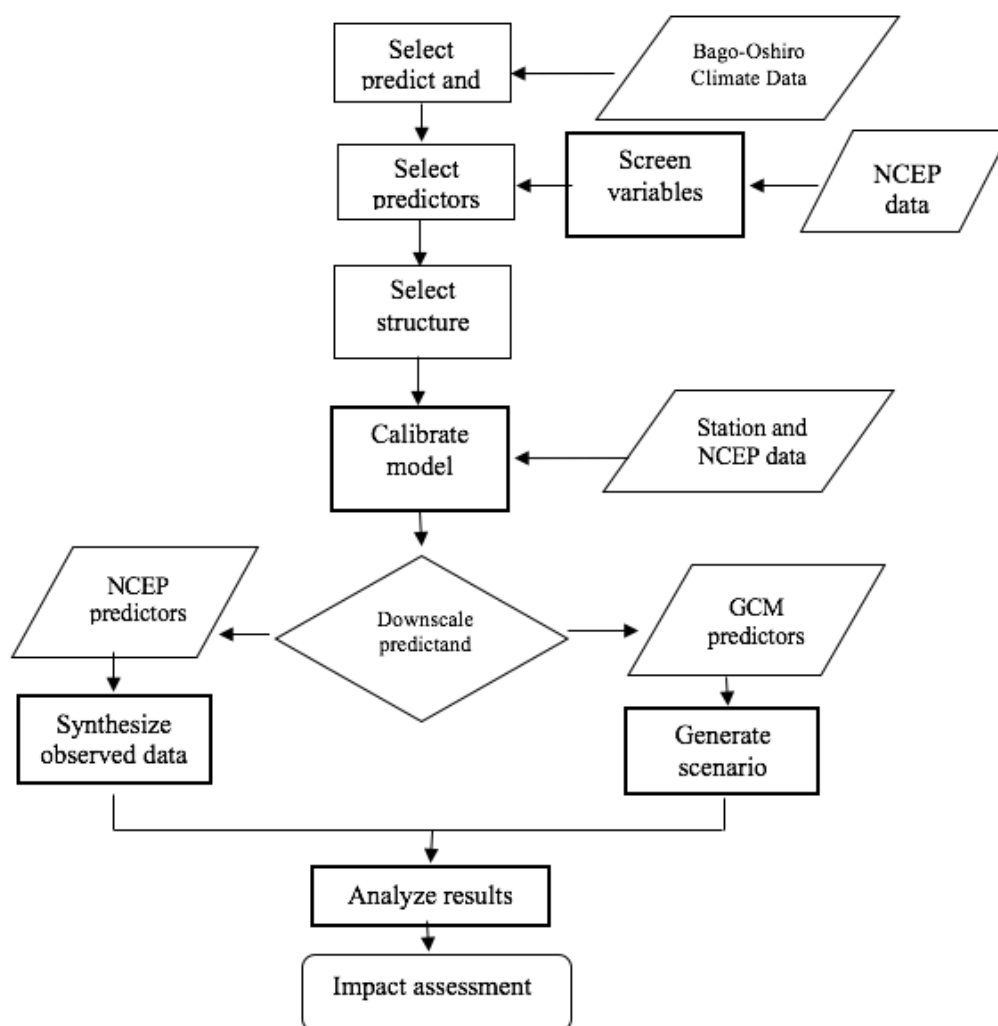


Figure 2. SDSM Climate Scenario Generation Process

Source : Wilby et al., 2002

Predictor variables were carefully selected based on a correlation analysis with predictand variables over a 12-month period, using a 95% confidence level. The chosen predictors were also evaluated for their conceptual and physical relevance to the local weather site. Table 1 demonstrates a strong correlation between these predictors and the predictands at the local weather station in Bago Oshiro. For minimum temperature (T_{min}), eight out of twenty-six potential predictors showed high correlation, including p , z , p_{th} , $p5_f$, 850 hPa, $p8th$, $s500$, $s850$, and $temp$. For maximum temperature (T_{max}), eight out of twenty-six identified predictors were highly sensitive in downscaling, namely: $slpg$, p , p_{th} , $p500$, $p5th$, $p5zh$, $s850$, $shum$, and $temp$. For precipitation,

seven out of twenty-six predictors exhibited high correlation with the predictand, specifically: slpg, p, u, p5, p500, p5zh, p8th, and p8zh.

Table 1. List of predictors from NCEP and CGCM3 datasets and selected predictors which correlates highly to each predictand.

| Predictors Code | Description | TMIN | Predictands TMAX | RAIN |
|--------------------|----------------------------|------|---------------------|------|
| Slpg | Mean sea level pressure | | X | X |
| p f | 1000 hPa Wind speed | | | |
| p u | 1000 hPa U-component | | | X |
| p v | 1000 hPa V-component | | | |
| p z | 1000 hPa Vorticity | X | | |
| p_th | 1000 hPa Wind direction | X | X | |
| p_zh | 1000 hPa Divergence | | | |
| p5_f | 500 hPa Wind speed | X | | |
| p5_u | 500 hPa U-component | | | X |
| p5_v | 500 hPa V-component | | | |
| p5_z | 500 hPa Vorticity | | | |
| p500 | 500 hPa Geopotential | | X | X |
| p5th | 500 hPa Wind direction | | X | |
| p5zh | 500 hPa Divergence | | X | X |
| p8_f | 850 hPa Wind speed | | | |
| p8_u | 850 hPa U-component | | | |
| p8_v | 850 hPa V-component | | | |
| p8_z | 850 hPa Vorticity | | | |
| p850 | 850 hPa Geopotential | X | | |
| p8th | 850 hPa Wind direction | X | | X |
| p8zh | 850 hPa Divergence | | | X |
| s500 | 500 hPa Specific humidity | X | | |
| s850 | 850 Specific humidity | X | X | |
| Shum | 1000 hPa Specific humidity | | X | |
| Temp | Temperature at 2m | X | X | |
| Prcp | Accumulated precipitation | | | |

2.2 Groundwater Modelling using BROOK90 Hydrological Model

First, hydrologic secondary data -- the gage height and water discharge gathered at the office of Materials Quality Control and Hydrology Division, Department of Public Works and Highways (DPWH), Davao City. The office takes charge of monitoring the streamflow of the said watersheds that measures the gage height of the water level three times a day. Streamflow data were monitored from 1980 up to the present.

Second, the next underlying process is the land cover analysis in which both normalized difference vegetation index (NDVI I4.7) and ArcGIS software were used to process reclassified land cover. These two processes are vital in determining the water budget.

The water budget is generated using the BROOK90 hydrologic model. Water budget is used to simulate daily evaporation and soil-water movement using a process-oriented approach for a single forest stand/site or a small watershed, with some provision for runoff (streamflow) generation by different flow paths (Federer et al. 2003). To account for varying land cover across the two watersheds, four simulation runs were conducted, each using parameter values tailored to a specific land cover classification. The generated simulated flow is the average of four land cover types. Precipitation is a function of streamflow, evaporation loss, and deep seepage. Datasets were divided into calibration period and validation period. Results were subjected to sensitivity analysis in order to determine the changes in the value of parameters and changes in structure (Combalicer, 2010).

BROOK90 is particularly beneficial for detailed investigations of soil water dynamics and evapotranspiration at a localized scale, as demonstrated by Vorobeyskii (2020) who utilized it with new R functionalities to estimate vertical water fluxes within the soil-water-plant system of a single site or a small catchment (under 100 km²). Furthermore, BROOK90 offers an automated framework for simulating water balance at any given location. However, there other hydrological software alternatives like SWAT (Kiniry, 2012) that represents a simplified groundwater representations and lateral flow limitations.

Figure 3 shows the meteorological and hydrological stations within the study area. Meteorological inputs are the simulated climate data (daily precipitation, temperature maximum, temperature minimum, and sunshine duration) generated from SDSM.. The PAGASA weather station is located at 07°04' 06" latitude and 125°27'99" longitude (Figure 3). Ten (10) years streamflow data were taken in both Talomo River and Lipadas River as monitored and archived by the DPWH in Davao City. The regional office of the Department of Environment and Natural Resources Office (DENR XI), also located in Davao City, was the source of the maps and shapefiles employed in this research.

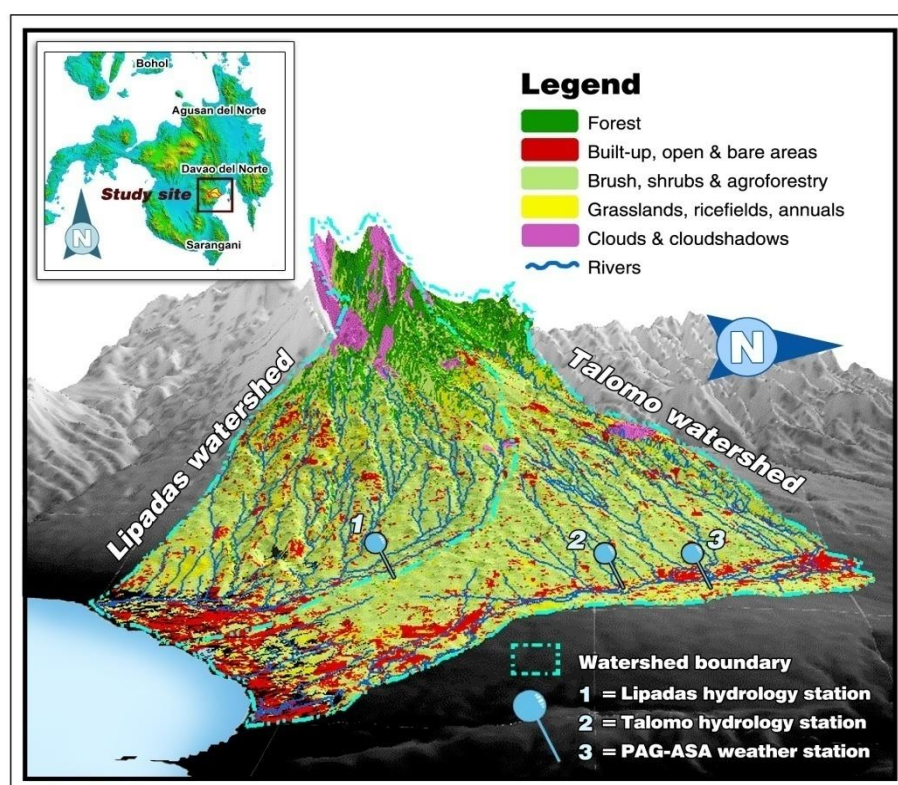


Figure 3. Land cover map of Talomo-Lipadas, PAGASA weather station, and hydrology station

The BROOK90 hydrological model requires six parameters: flow, location, drainage, canopy, soil, and initial conditions. These parameters were carefully adjusted to calibrate the model for accurate discharge simulation in the two watersheds. A sensitivity analysis particularly RMSE and Nash-Sutcliffe were performed on the measured and simulated discharges to evaluate model fit. Additionally, monthly and yearly water balances analyses were conducted. Figure 4 illustrates these essential BROOK90 parameters.

Location parameters. This section describes site-specific parameters used in the study, focusing on location and environmental factors. For the Talomo site, the latitude is 7.08, while for Lipadas it is 7.09. The degree slope for evapotranspiration is 34.45 in Talomo and 34.23 in Lipadas. A snow-rain transition temperature of -0.5 and a degree day melt factor for open land of 1.5 were used. Relative height and relative leaf area index (an array of ten day-of-year and relative LAI values between 0 and 1) are also specified. Finally, (DURATN), representing the average duration of daily precipitation per month, is included as a parameter.

Flow parameters. In this model, water infiltration is controlled by two parameters: INFEXP and IDEPTH. Setting both to zero simulates a basic top-down infiltration process. Specifically, IDEPTH controls the number of soil layers that receive infiltrated water, while INFEXP determines the distribution of that water within the soil layers. Table 1 represents the final values used for flow meter.

Table 1. Final Values for Flow Parameter

| Parameters | Description | Range | Final Values |
|------------|---|-------------|--------------|
| IDEPTH | Depth over which infiltration is distributed | > 0 | 1,000 |
| INFEXP | Infiltration exponent that determines the distribution of infiltrated water with depth, (f) | 0 - 1.0 | 1.0 |
| IMPERV | Fraction of the soil surface that is impermeable and always routes water reaching it directly to streamflow | 0 - 1 | 0.01 |
| BYPAR | Bypass flow from deeper layers | 0 - 1 | 0 |
| QDEPTH | Soil depth for SRFL calculation (mm) | ≥ 0 | 1,000 |
| QFPAR | Fraction of the water content between field capacity (THETAF) and saturation (THSAT) at which the quick flow fraction is 1, (f) | 0.2 - 5 | 1 |
| QFFC | Quick flow fraction for SRFL and BYFL at THETAF, (f) | 0.02 – 0.3 | 0.05 |
| LENGTH | Slope length for downslope flow (m) | ≥ 0 | 10000 |
| DSLOPE | Downslope, (deg) | ≥ 0 | 4 |
| DRAIN | Multiplier between 0 and 1 of drainage from the lowest soil layer, (f) | 0 - 1 | 0.01 |
| GSC | Fraction of groundwater storage (GWAT), that is transferred to groundwater (GWFL) and deep, seepage (SEEP) each day, (f) | 0.005 – 0.5 | 0.003 |
| GSP | Fraction of groundwater (discharge, (f) | ≥ 0 | 0 |

Canopy parameters: Several parameters related to the forest canopy and land surface are critical for determining how quickly trees transpire as reflected in table 2. These include the surface albedo (reflectivity) under both snow-free (ALB) and snow-covered (ALBSN) conditions, which may be known for specific locations. The relative density of tree roots (ROOTDEN) is another important factor. Additionally, the fraction of plant resistance located within the xylem tissue (FXYLEM) plays a role, as this parameter, in conjunction with ROOTDEN, controls the amount of transpiration occurring in each soil layer. Finally, the maximum height of the forest canopy (MAXHT) and the maximum projected

leaf area index (MAXLAI) are considered. MAXLAI is influenced by the density of the forest at a given site.

Table 2. Final Values for Canopy Parameter

| Parameters | Description | Range of Values | Final Values |
|------------|--|-----------------|--------------|
| ALB | Albedo | 0.1 – 0.3 | 0.23 |
| ALBSN | Surface reflectivity without and with snow on the ground (f) | 0.1 – 0.9 | 0.35 |
| KSNVP | Multiplier to reduce snow evaporation, arbitrary (f) | 0.2 – 2.0 | 0.3 |
| ZOG | Ground surface roughness (m) | ≥ 0.001 | 0.02 |
| MAXHT | Maximum canopy height for the year (m) | > 0.01 | 50 |
| MAXLAI | Maximum projected LAI for the year (m^2/m^2) | > 0.00001 | 6 |
| MXRTLN | Maximum length of fine roots per unit ground area m/m^2) | 1700 – 11000 | 3500 |
| MXKPL | Maximum plant conductivity ($\text{mmd}^{-1} \text{Mpa}^{-1}$) | 5-30 | 8 |
| FXYLEM | Fraction of the internal plant resistance to water flow that is in the xylem (f) | 0 – 0.99 | 0.5 |
| CS | Ratio of projected stem area index (SAI) to HEIGHT (f) | ≥ 0 | 0/35 |
| PSICR | Minimum plant leaf (Mpa) | -15 – 20 | -2 |
| GLMAX | Maximum leaf conductance (cm/s) | 0.2 – 2.0 | 0.57 |
| LWIDTH | Average leaf width (m) | > 0.01 | 0.08 |
| CR | Extinction coefficient for photosynthesis-active radiation in the canopy (f) | 0.5 – 0.7 | 0.6 |

Source: Combalicer, 2010

In modelling climate change impacts on hydrological processes, the canopy parameter variables were run four (4) times per land cover types (table 3). Each canopy parameter was adjusted (Federer, 2014) to obtain reasonable values per land cover type. The four land cover types represent the simulated flow of the area.

Table 3. Final Values for Each Land Cover Type

| Parameters | Forest | Brush | Grassland | Bare |
|------------|--------|-------|-----------|-------|
| ALB | 0.25 | 0.62 | 0.09 | 0.16 |
| ALBSN | 0.23 | 0.5 | 0.45 | 0.35 |
| KSNVP | 0.3 | 1 | .3 | .3 |
| ZOG | 0.02 | 0.02 | 0.02 | 0.02 |
| MAXHT | 30 | .3 | 10 | 10 |
| MAXLAI | 6 | 3 | 6 | 6 |
| MXRTLN | 3500 | 110 | 2000 | 100 |
| MXKPL | 15 | 8 | 8 | 8 |
| FXYLEM | 0.5 | 0 | 0.5 | 0.5 |
| CS | 0.035 | 0.035 | 0.035 | 0.035 |
| PSICR | -2 | -2 | -2 | -2 |
| GLMAX | 0.53 | 1.1 | 0.5 | 0.5 |
| LWIDTH | 0.1 | 0.1 | 0.05 | 0.05 |
| CR | 0.6 | 0.7 | 0.6 | 0.6 |

Soil parameters. This section describes soil profile and water property parameters used in the BROOK90 model, emphasizing the influence of the number of soil layers as shown in table 4. NLAYER defines the number of soil layers, while THICK specifies the thickness of each layer. Key parameters include: hydraulic conductivity at field capacity (KF, in mm/d), volumetric water content at field capacity (THETAF), and matric potential at field capacity (PSIF). RELDEN represents the relative root density per unit volume (m^3/m^3), STONEF is the stone volume fraction, and WETINF denotes the wetness at the dry end of the near-saturation range. Finally, PSIM specifies the initial matric soil water potential (kPa) for each layer.

Table 4. Final Values for Soil Parameter

| Layer No | Soil Depth (THICK), mm | Stone volume fraction (STONE), f | Matrix potential (PSIF), kPa | Volumetric water content (THETAF), m^3/m^3 | Matrix porosity (THSAT), m^3/m^3 | Negative slope of the log psi (BEXP) | Hydraulic conductivity (KF), mm/d |
|----------|------------------------|----------------------------------|------------------------------|--|------------------------------------|--------------------------------------|-----------------------------------|
| 1 | 200 | 0 | -6.0 | 0.397 | 0.60 | 7.75 | 4.9 |
| 2 | 400 | 0 | -7.7 | 0.425 | 0.60 | 11.4 | 4.3 |
| 3 | 600 | 0 | -7.7 | 0.425 | 0.60 | 11.4 | 4.3 |
| 4 | 800 | 0 | -7.7 | 0.425 | 0.60 | 11.4 | 4.3 |
| 5 | 1000 | 0 | -6.5 | 0.433 | 0.60 | 10.4 | 4.2 |

Source: Combalicer, 2010

Fixed parameters. These are constant values established based on a range of sources, and there no recommendations provided for altering them.

Initial parameters. All the parameters can be configured to a value of 0, with the exception of PSIM, which may be -10 kPa. Typically, an initializing period, often spanning a year, is executed to mitigate the impact of initial values. In BROOK90 this process is facilitated through the ‘number of initialize days’ feature on the main screen. Each parameter's values were properly adjusted to accurately measure and calibrate the discharges in the two watersheds. Results of measured and simulated water discharges were subjected to sensitivity analysis to determine the model's fitness. Water balance analysis was then simulated monthly and yearly.

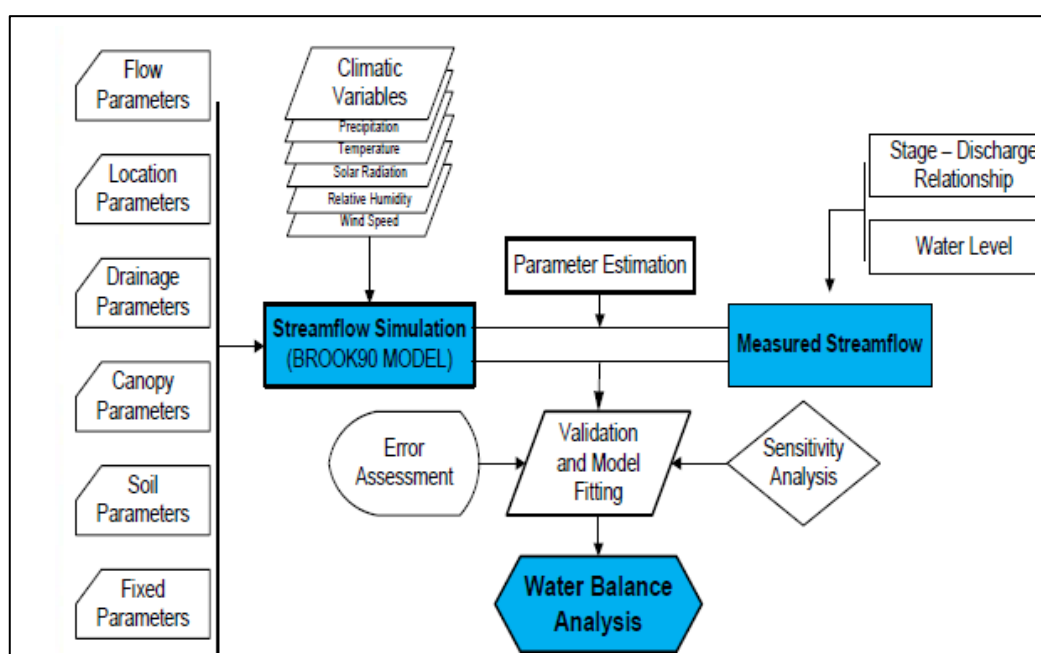


Figure 4. Parameters used in BROOK90 Model

Source: Combalicer, 2010

3. RESULTS AND DISCUSSION

3.1 Local Climate Projection using Statistical Downscaling Method (SDSM)

Statistical Downscaling Model (SDSM) was employed to generate present and future climate scenarios centered on the three time slice periods at 2020 (2011-2040), 2050 (2041-2070) and 2080 (2071-

2100). Calibration and validation processes were carried out to identify the most fitting model for projecting climate scenarios. Model calibration involved the creation of monthly structured models, utilizing twelve distinct regression models, each representing a specific month and incorporating various parameters.

The calibration process spanned a period of 20 years (1976-1995), while model validation encompasses 12 years (1989-2000) as shown in table 5. The data sets were divided based on the methodologies outlines by Kozak (2003) and Fattha (2012) which advocate for the implementation of cross-validation and double cross validation to enhance the reliability of information derived from the data. In both calibration and validation figures, the line graph demonstrates a strong agreement of the observed and simulated data of minimum and maximum temperature and precipitation.

Improved concordance was achieved due to the minimal disparity between the observed data and residual or simulated data. The calculated RMSE and MAE were lower in minimum (Tmin) and maximum temperature (Tmax) compared to the rainfall during the calibration and validation processes.

Table 5. Summarize model evaluation criteria

| | Rainfall | | TMIN | | TMAX | |
|------|-------------|------------|-------------|------------|-------------|------------|
| | Calibration | Validation | Calibration | Validation | Calibration | Validation |
| RMSE | 13.12 | 14.81 | 1.57 | 1.62 | 1.32 | 1.49 |
| MAE | 7.57 | 8.32 | 1.17 | 1.16 | 0.96 | 1.07 |
| E | -0.0173 | 0.0237 | 0.0853 | 0.1220 | 0.0902 | 0.1212 |

Table 6 presents the projected minimum temperatures (Tmin) under future climate scenarios of 2020, 2050, and 2080 and their increase/decrease relative to observed values (Figure 5). The Tmin fluctuates slightly but generally show an increasing trend over time. Some months like March, April, and November show slight cooling in later projections (2080), while other, May and July exhibit warming temperature. Higher minimum temperatures are observed in March, April, May, June, September and October. While July and August have lowest Tmin. Global climate models under A2 scenario, minimum temperatures will increase (IPCC, 2021). Higher minimum temperatures can disrupt plant growth cycles, particularly in tropical and subtropical regions (Hatfield and Prueger, 2015). Warming nights reduce cooling periods for crops,

impacting yield quality and production (Rosenzweig et al., 2001). Countries dependent on rain-fed agriculture may face drought risks due to increased evaporation (Christensen et al., 2007). Figure 5 shows the graphical representation on the trends over time.

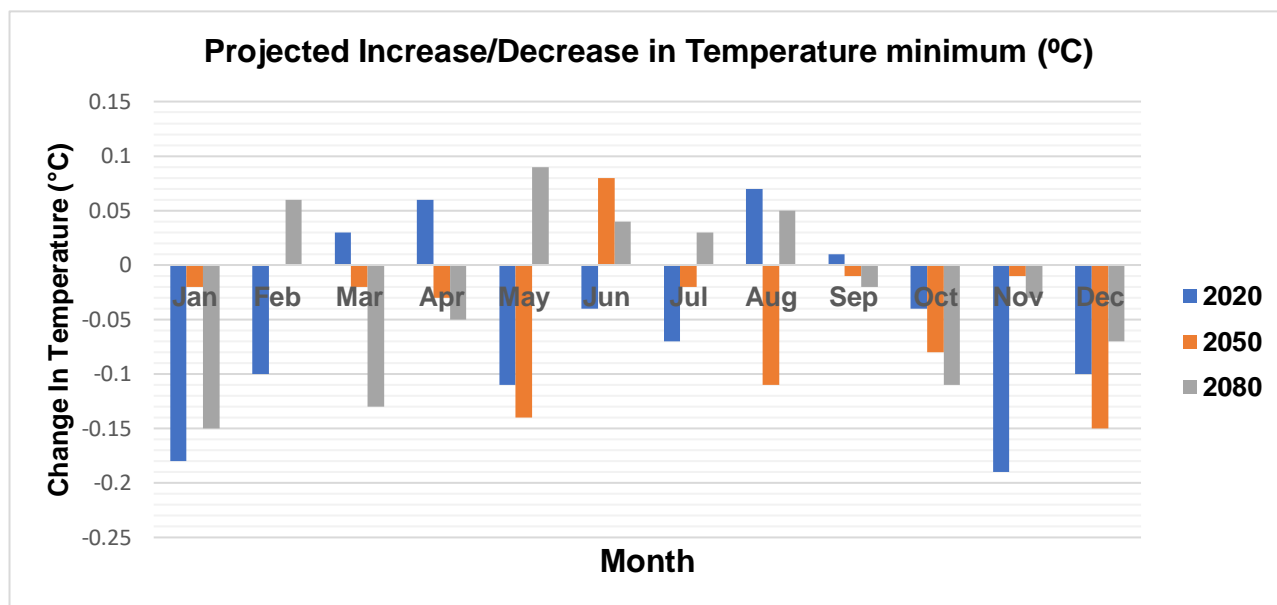


Figure 5. Projected changes in mean monthly minimum temperature (°C)

Table 6. Mean monthly comparison and rate of change (increase/decrease) on minimum temperature

| Month | Observed data | TEMPERATURE MINIMUM | | | | | |
|-------|---------------|---------------------|-------|-------|-------------------|--------------|--------------|
| | | Centigrade (°C) | | | Increase/Decrease | | |
| | | 2020 | 2050 | 2080 | 2020 | 2050 | 2080 |
| Jan | 21.39 | 21.20 | 21.37 | 21.24 | -0.18 | -0.02 | -0.15 |
| Feb | 21.78 | 21.68 | 21.78 | 21.84 | -0.10 | 0.00 | 0.06 |
| Mar | 22.14 | 22.17 | 22.12 | 22.01 | 0.03 | -0.02 | -0.13 |
| Apr | 21.93 | 21.99 | 21.90 | 21.88 | 0.06 | -0.03 | -0.05 |
| May | 22.05 | 21.94 | 21.91 | 22.15 | -0.11 | -0.14 | 0.09 |
| Jun | 21.38 | 21.34 | 21.46 | 21.42 | -0.04 | 0.08 | 0.04 |
| Jul | 20.89 | 20.81 | 20.86 | 20.91 | -0.07 | -0.02 | 0.03 |
| Aug | 21.07 | 21.14 | 20.96 | 21.11 | 0.07 | -0.11 | 0.05 |
| Sep | 21.09 | 21.10 | 21.08 | 21.07 | 0.01 | -0.01 | -0.02 |
| Oct | 21.07 | 21.03 | 20.98 | 20.96 | -0.04 | -0.08 | -0.11 |
| Nov | 21.39 | 21.20 | 21.38 | 21.36 | -0.19 | -0.01 | -0.03 |
| Dec | 21.21 | 21.10 | 21.06 | 21.14 | -0.10 | -0.15 | -0.07 |

Figure 6 depicts the projected mean monthly maximum temperature (Tmax) for Talomo-Lipadas Watersheds. There is a most striking feature of the projected temperatures for both 2020 and 2050's which have generally higher Tmax from the observed temperatures across all months. Table 7 depicts in numerical values on the increase and decrease of Tmax which clearly indicates a future warming trend in the said watersheds. The degree of warming appears to intensify from the 2020s to the 2050s, suggesting a progressive increase in Tmax over time as climate impacts become more pronounced. While, the overall trends in warming, the figure as well as the numerical increase/decrease as shown on table 7 an increases varies across different months. It is crucial to examine the seasonal changes to understand their potential impacts on specific ecological processes and human activities. For instance, the months of March to May exhibit the highest projected temperatures which could exacerbate drought conditions. Increased Tmax can lead to higher evapotranspiration rates, potentially reducing soil moisture and impacting water availability for both natural ecosystems and human use. Parmesan, C, and Yohe, G (2023) stated that rising temperatures can disrupt ecological processes, affecting species distribution, phenology, and ecosystem productivity. Warmer temperatures can also favour of invasive species and increase the risk of pest and disease outbreak. Agriculture is highly sensitive to temperature changes. Increased maximum temperatures can reduce crop yields, particularly for heat-sensitive crops. Change in temperature patterns can also affect the timing of planting and harvesting, potentially disrupting agricultural practices (Tubiello, F.N. et al. 2007).

Subsequently, this potential temperature increase would bring immense changes to the hydrological processes and vegetation responses. Plants are highly dependent on climatic conditions hence, the “sponge” effect of the forest will be affected with the potential increase in temperature. This will have implication to the climate-dependent sectors especially among domestic water users, agricultural water users, commercial and industrial users, among others.

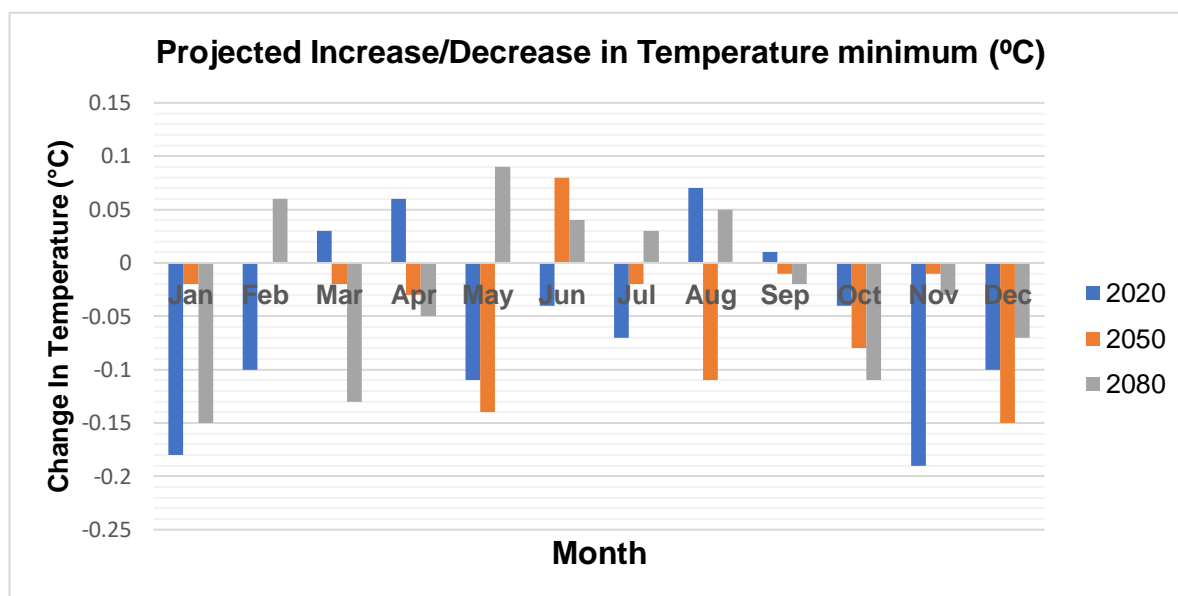


Figure 6 . Projected changes in mean monthly maximum temperature (°C)

Table 7. Mean monthly comparison and rate of change (increase/decrease) on maximum temperature

| Month | Observed data | TEMPERATURE MAXIMUM | | | | | |
|-------|---------------|---------------------|-------|-------|-------------------|--------------|--------------|
| | | Centigrade (°C) | | | Increase/Decrease | | |
| | | 2020 | 2050 | 2080 | 2020 | 2050 | 2080 |
| Jan | 30.57 | 30.67 | 30.47 | 30.64 | 0.10 | -0.10 | 0.07 |
| Feb | 30.86 | 30.74 | 30.86 | 30.77 | -0.12 | 0.00 | -0.09 |
| Mar | 31.49 | 31.54 | 31.60 | 31.46 | 0.05 | 0.11 | -0.03 |
| Apr | 32.06 | 32.13 | 32.14 | 32.15 | 0.07 | 0.08 | 0.09 |
| May | 31.65 | 31.71 | 31.65 | 31.75 | 0.06 | 0.00 | 0.11 |
| Jun | 30.94 | 30.97 | 31.04 | 31.01 | 0.03 | 0.10 | 0.07 |
| Jul | 30.57 | 30.52 | 30.69 | 30.66 | -0.06 | 0.12 | 0.08 |
| Aug | 30.45 | 30.45 | 30.50 | 30.46 | 0.00 | 0.04 | 0.01 |
| Sep | 30.63 | 30.63 | 30.57 | 30.61 | -0.01 | -0.07 | -0.03 |
| Oct | 30.94 | 30.93 | 31.00 | 30.88 | -0.02 | 0.06 | -0.06 |
| Nov | 31.11 | 31.19 | 31.12 | 31.10 | 0.08 | 0.01 | -0.01 |
| Dec | 30.56 | 30.39 | 30.45 | 30.45 | -0.17 | -0.11 | -0.10 |

As to precipitation, the three slice time periods 2020, 2050 and 2050 show consistent more and heavy rain with a remarkable increase in January. All three time slice periods show significant increase of 38.79%, 28.15% and 24.84%, respectively compared to the observed data.

The results of this study, based on statistical downscaling, contradicted PAGASA's (2011, p. 42) future rainfall projections obtained via dynamical downscaling. According to PAGASA's medium-range emission scenario, rainfall was not expected to surpass 300 mm in 2020 and 2050, a finding that differs from the current analysis. The statistical downscaling method has projected an increase of over 300mm (about 11.81 in) specifically for June (335 mm) especially in the 2050 sliced period. This validation process will identify the most representative models for the region. Recognizing the inherent uncertainties in climate projections, as acknowledged by the IPCC, necessitates ongoing efforts to refine modelling techniques and improve the reliability of local-scale predictions.

Analysis indicates a likely shift towards a wetter season in the watersheds (Table 8). Notably, several months are predicted to have significantly higher rainfall volumes, with potential increases reaching 42.87%. This necessitates proactive disaster risk management strategies, including the development of effective early warning systems for floods and landslides. The agricultural sector must respond by adapting cropping patterns and choosing appropriate crops. Conversely, industries like hydroelectric power plants can capitalize on the increased water availability.

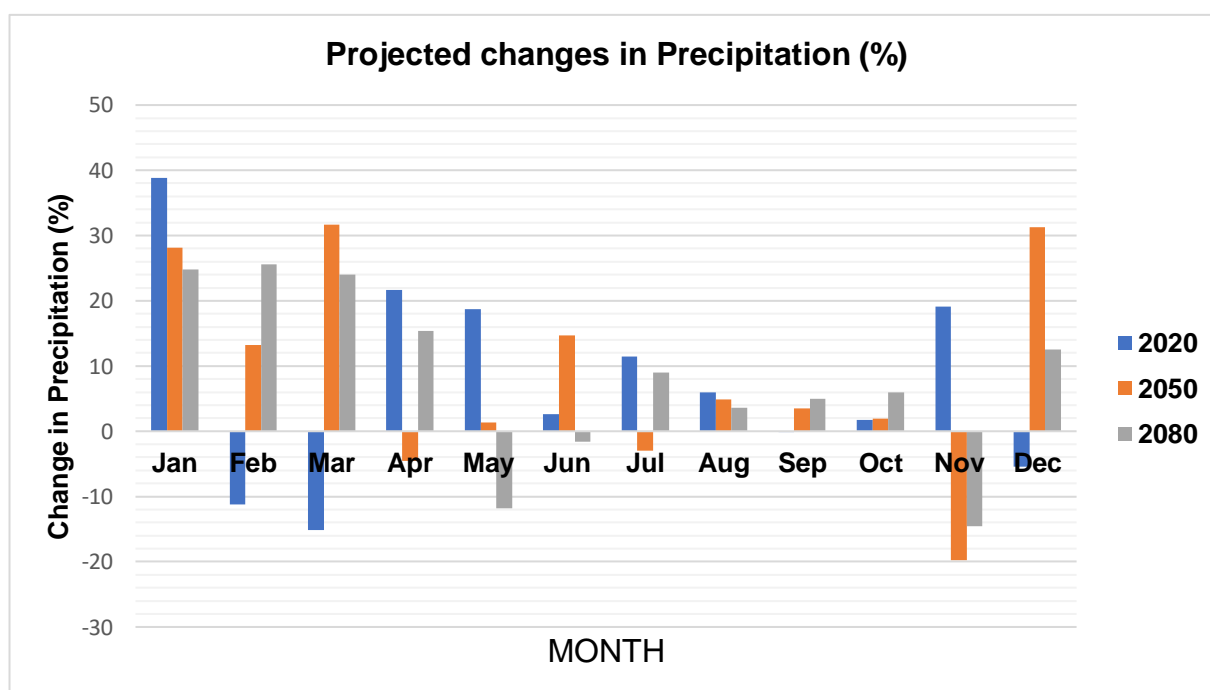


Figure 7. Projected changes in precipitation (%)

Table 8. Mean monthly comparison and percent change on amount of precipitation

| Month | Observed data | PRECIPITATION | | | | | |
|-------|---------------|---------------|------|------|-----------------------|---------------|---------------|
| | | (mm) | | | Increase/Decrease (%) | | |
| | | 2020 | 2050 | 2080 | 2020 | 2050 | 2080 |
| Jan | 128 | 178 | 164 | 160 | 38.79 | 28.15 | 24.84 |
| Feb | 81 | 72 | 91.8 | 102 | -11.18 | 13.25 | 25.62 |
| Mar | 101 | 86 | 133 | 126 | -15.17 | 31.62 | 23.97 |
| Apr | 170 | 207 | 162 | 196 | 21.68 | -4.59 | 15.38 |
| May | 276 | 327 | 279 | 243 | 18.73 | 1.35 | -11.85 |
| Jun | 292 | 300 | 335 | 288 | 2.63 | 14.65 | -1.63 |
| Jul | 217 | 241 | 210 | 236 | 11.49 | -2.94 | 9.04 |
| Aug | 248 | 262 | 260 | 256 | 5.97 | 4.88 | 3.57 |
| Sep | 219 | 219 | 227 | 230 | -0.10 | 3.46 | 4.95 |
| Oct | 210 | 213 | 214 | 222 | 1.70 | 1.97 | 5.94 |
| Nov | 177 | 211 | 142 | 151 | 19.15 | -19.73 | -14.52 |
| Dec | 141 | 134 | 186 | 159 | -5.42 | 31.26 | 12.55 |

3.2 Modelling Hydrologic Responses using BROOK90 Hydrological Model

This section measured how changing climate influences the hydrological processes with the given land cover and other associated parameters. In projecting water quantity, this paper assumes that no changes shall be made to the land cover. The watersheds comprise of 15 land covers and are further narrowed down to four major land cover classifications. As shown on figure 3, the area is dominated with Brushland (agroforestry, shrubs, and brushes) constituting 23313.9 hectares (59.10%); Bare lands (urban, harvested rice fields, open areas, and exposed soil) constituting 5623.9 hectares (14.26); forest constitutes 4,864.6 hectares (12.33%); and Grassland (rice fields and wastelands) constitutes another 4,025.5 (10.2%).

One focus of this study is the quantification of groundwater (seepage) since it is deemed essential in analyzing water supply as water is being mined from the groundwater. Essential to this modelling is the calibration and validation process. It is pre-requisite for the fitness of the model where all predictors

need to be fit, and fitness will only be acceptable when these will be subjected further to statistical analysis where values are acceptable (RMSE and Nash Sutcliffe).

This study utilized streamflow data from two distinct watersheds, the Talomo and Lipadas watershed. Each dataset was split into two parts for model calibration and validation. Climate data for both watersheds were derived from a single source: the Bago Oshiro Agrometeorological Station, situated within the Talomo Watershed. The average annual precipitation was 2873.83 mm during the calibration period and 2858.8 mm during the validation period.

Average annual streamflow varied between calibration and validation periods for both watersheds. In the Talomo watershed, streamflow was 1251.70 mm during calibration and increased to 1412.45 mm during validation. The Lipadas watershed saw a decrease, from 1088.83 mm during calibration to 907.03 mm during validation.

A high coefficient of determination (R^2) value as shown in table 9 and figure 8 and 9 indicates a strong annual relationship between measured and simulated streamflow. This metric (ranging from 0 to 1) reflects the model's predictive skill, quantifying the proportion of streamflow variability captured. Positive Nash-Sutcliffe coefficients further validate the model's performance. However, the model's sensitivity was insufficient to accurately simulate monthly and daily streamflow. Despite this limitation, considering the limited availability of climate and streamflow data in the region, this simulation represents the best achievable outcome. Results for calibration and validation were obtained by averaging across four land cover types, employing appropriate parameters, especially for canopy characteristics, as suggested by the BROOK90 model (Federer, 2002).

Table 9. BROOK90 model simulation in Mt. Talomo-Lipadas Watersheds

| Watersheds | Performance criteria | Calibration | Validation |
|------------|----------------------|-------------|------------|
| Talomo | R^2 | 0.979 | 1.000 |
| | Nash-Sutcliffe | 0.845 | 0.621 |
| Lipadas | R^2 | 1.000 | 1.000 |
| | Nash-Sutcliffe | 0.622 | 0.836 |

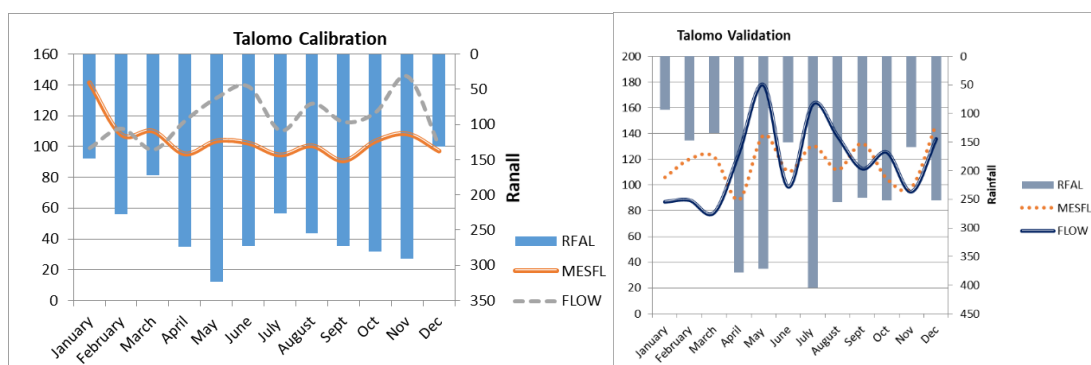


Figure 8. Calibration Period for Talomo Watershed (left) and Validation Period for Talomo Watershed (right)

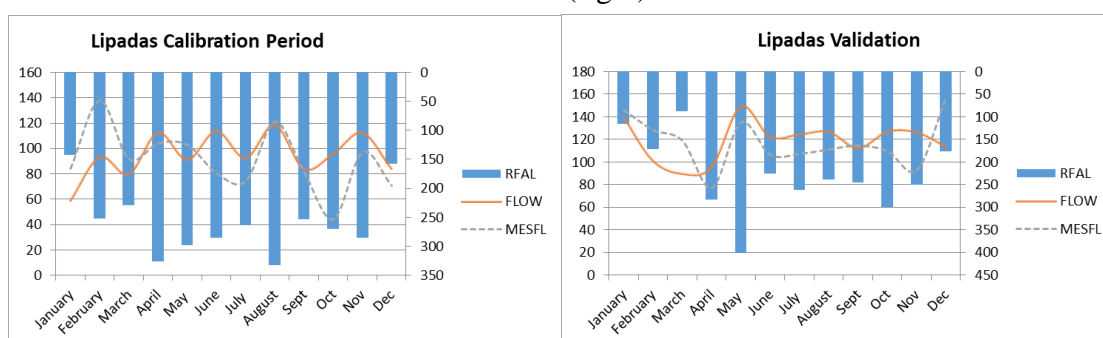


Figure 9. Calibration Period for Lipadas Watershed (left) and Validation Period for Lipadas Watershed (RFAN- rainfall; MSFL- measured flow; FLOW- simulated flow)

Considering the limited availability of observed streamflow and climate data, the model validation achieved a higher coefficient of determination, indicating a better fit to observed data than the calibration period for both watersheds.

3.3 Projected Recharge (Seepage) of Talomo-Lipadas Watersheds

In the BROOK90 model, recharge, the water withdrawn primarily by the Davao Water District to supply 99% of the urban population, is calculated as precipitation minus evaporation and flow. Precipitation is the primary source of all water in the terrestrial phase of the hydrologic cycle (Satterlund, 1972, cited in Combalicer, 2010).

Analysis of recharge data from 1997 to 2006 across the two watersheds revealed an annual average of 134.06 million cubic meters (MCM). The lowest flow months were typically observed in March, while July experienced the highest flows.

Over the coming decades as shown in table 10 and figure 9, recharge is projected to decline. By 2020, a reduction of -18.63% (25.1 MCM) is expected, with low flow from April to December, reaching a minimum of -55.29% (3.98 MCM) in April. In 2050, the reduction is projected to be -23.08% (31.07 MCM) continuously from March to December. By 2080, the decline reaches -25.84% (34.79 MCM), with low flow spanning the same period.

The results indicate a strong sensitivity of groundwater recharge in the Talomo-Lipadas Watersheds to climate change. A relatively small rise in maximum temperature, ranging from 0.10°C to 0.17°C, is sufficient to negatively impact water availability for recharge.

The projected decline in groundwater recharge, despite increased rainfall, is a serious concern for future water supplies. Reductions are projected to reach 18.63% by 2020, 23.08% by 2050, and 25.84% by 2080, highlighting the urgency of addressing this issue.

The above findings are concurrent to a study conducted by Zektser and Loaiciga, (1993); Bear and Cheng (1999) where climate has the potential effects on the quantity and quality of groundwater. Climate change and variability will have numerous effects on recharge rates and mechanism (Vacarro, 1992; Green et al., 2007a; Kunzewicz et al., 2007; Aguilera and Murillo, 2009). The impact of climate change on groundwater recharge is a subject of ongoing research, with many studies predicting declines (Herrera-Pantoja and Hiscock, 2008). Kruger et al. (2001) provide an example, projecting a potential 30% reduction in a lowland aquifer in Germany.

The decline in groundwater recharge despite increased rainfall is attributed to a significant increase in evapotranspiration (ET) (Fasullo et al., 2015) Rising temperatures, associated with climate change, have led to higher potential ET. Additionally, (Morris 2017) changes in land cover, such as deforestation, have reduced canopy interception and increased soil evaporation. (Famiglietti, J. S. (2014). Soil moisture indicates that a larger proportion of rainfall is being lost through ET, leaving less water available for infiltration and recharge. This is supported by process-based modelling, which shows a strong correlation between increased temperatures and reduced recharge, even with increased precipitation.

The dynamic nature of groundwater recharge, driven by precipitation variability, can have cascading effects on groundwater systems. These include impacts on aquifer yield and discharge, along with potential shifts in flow regimes, such as the conversion of gaining streams to losing streams and adjustments to groundwater divides. Also, Green et al. (2007) simulated recharge is highly dependent on the combination of soil and vegetation type.

Land use and land cover changes (LULC) significantly influence groundwater storage by altering key hydrological processes such as infiltration, evapotranspiration, and runoff. In the Talomo-Lipadas Watersheds, the dominant land cover type is Brushland (59.10%), followed by Bare lands, Forest, and Grassland. Increase bare land cover contributes to higher surface run off, which not only reduces infiltration but also leads to soil erosion, further, reducing the watershed's ability to retain water. These land cover classifications play a crucial role in groundwater recharge (seepage) and, consequently, in the sustainability of water resources.

Also, in urbanized and bare land areas, impervious surface like roads, buildings, and compacted soil prevent water from infiltrating, as a result more precipitation is lost as surface run off rather than recharging groundwater reserves. Observed deforestation activities in the area disrupts the natural cycle of infiltration, reducing the capacity of soils to retain and slowly release into aquifers. Paul (2006) recharge is influenced by the type of land cover. Paul (2006) found out that there is notable variation of the groundwater recharge on the type of land use. The low groundwater recharge in settlements, a consequence of impervious surfaces and infrastructure, contrasts sharply with the high recharge rates in forested areas. This highlights the critical role of forests in maintaining groundwater supplies and the vulnerability of these resources to human development.

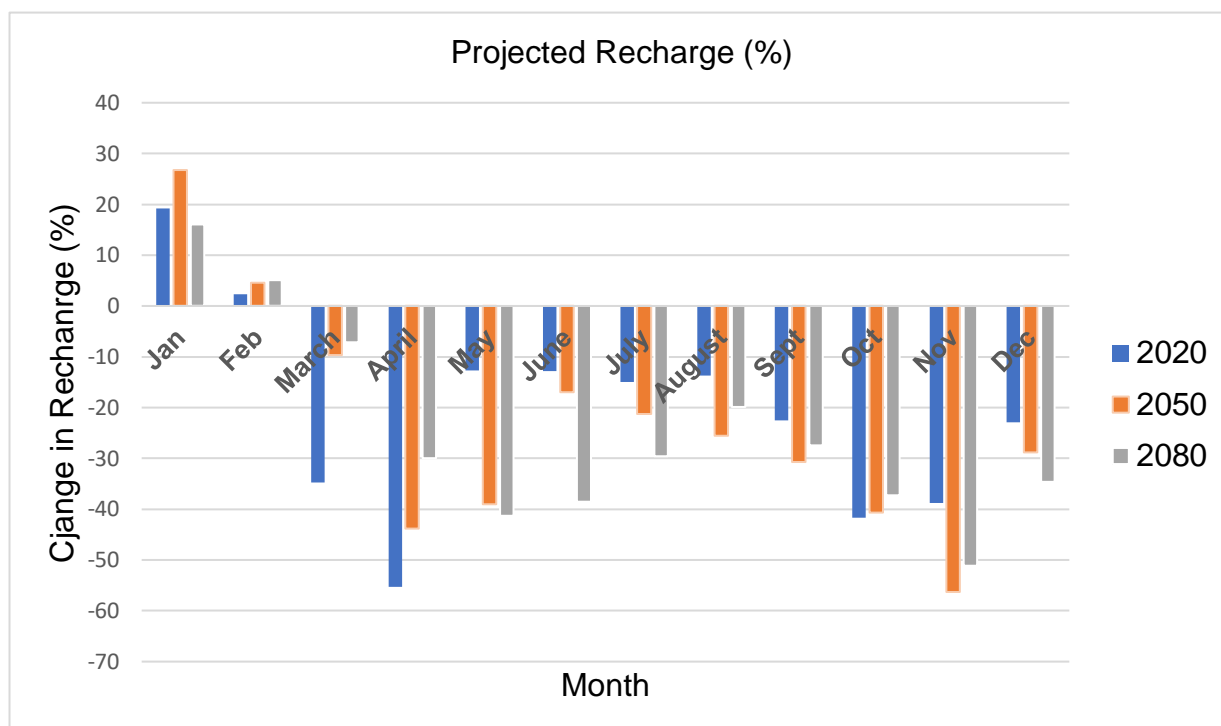


Figure 9. Recharge changes in 2020, 2050, and 2080 in percentage

Table 10. Recharge to groundwater expressed in Million Cubic Meter (MCM) in three time slice period for the two subwatersheds.

| Months | Recharge (MCM) | | | | % Increase/Decrease | | |
|--------|----------------|--------|--------|-------|---------------------|--------|--------|
| | OBS | 2020 | 2050 | 2080 | 2020 | 2050 | 2080 |
| Jan | 11.82 | 14.1 | 14.98 | 13.71 | 19.25 | 26.71 | 16 |
| Feb | 8.97 | 9.18 | 9.39 | 9.43 | 2.27 | 4.60 | 5.06 |
| March | 6.30 | 4.12 | 5.70 | 5.86 | -34.72 | -9.66 | -7.2 |
| April | 7.37 | 3.29 | 4.14 | 5.16 | -55.29 | -43.86 | -30.01 |
| May | 11.77 | 10.28 | 7.18 | 6.91 | -12.65 | -38.97 | -41.29 |
| June | 16.56 | 14.44 | 13.74 | 10.18 | -12.8 | -17.02 | -38.53 |
| July | 15.55 | 13.22 | 12.25 | 10.96 | -15.01 | -21.24 | -29.54 |
| August | 12.71 | 10.97 | 9.47 | 10.19 | -13.72 | -25.54 | -19.88 |
| Sept | 12.24 | 9.49 | 8.48 | 8.89 | -22.47 | -30.72 | -27.41 |
| Oct | 11.37 | 6.64 | 6.75 | 7.14 | -41.64 | -40.68 | -37.22 |
| Nov | 9.85 | 6.04 | 4.31 | 4.82 | -38.75 | -56.29 | -51.11 |
| Dec | 10.03 | 7.74 | 7.13 | 6.56 | -22.89 | -28.88 | -34.58 |
| Total | 134.6 | 109.50 | 103.53 | 99.81 | -18.63 | -23.08 | -25.84 |

Groundwater recharge (seepage) is strongly influenced by land cover. In this watershed, brushland is the predominant land cover, constituting 59.10% of the total area. Research by Paul (2006) has demonstrated the significant variation in groundwater recharge across different land uses. Specifically, settlement zones, due to extensive impervious surfaces and infrastructure, experience minimal recharge, whereas natural or

near-natural forested areas receive the highest levels. This highlights the critical role of forest vegetation in maintaining groundwater resources and the detrimental effects of anthropogenic activities on these systems.

4. CONCLUSIONS

This research directly addresses the need for local-level studies on climate change impacts, a call echoed internationally and nationally. Literature on this topic is limited, particularly in developing nations and specifically within the Philippines. In Davao City, the reality of climate change's effects on water resources, particularly groundwater availability, is evident. Using the Statistical Downscaling Method climate scenarios both minimum (T_{min}) and maximum temperatures (T_{max}) increases over time. Of greater concern is the projected rapid increase in precipitation. These results highlight the potential for both water shortages and increased risks of floods and landslides, requiring immediate attention from all sectors related to climate and water.

Using the BROOK90 hydrological software, it projects a decline in seepage due to the combined effects of climate change, land cover alterations, and other relevant parameters. The resulting monthly, annual, and time-slice recharge data provide valuable information for various stakeholders. This information will be crucial in designing, planning, and implementing water conservation strategies, especially for the Davao City Water District (DCWD) as they plan for future water sourcing to meet the needs of the city's expanding population.

Based on the compelling empirical evidence presented, the full integration of the downscaled, station-scale climate scenario is strongly recommended across all climate and water-related sectors within the Talomo-Lipadas Watershed. This information should be foundational to all planning and development initiatives, ensuring climate resilience and water security. Disaster risk reduction and management agencies should leverage these findings for proactive preparedness against potential extreme weather events. To enhance the robustness of future projections, expanding the weather station network and employing multi-model approaches for both climate downscaling and hydrologic modelling are essential for validation. Furthermore, maximizing recharge data collection is critical for developing a comprehensive, 100-year water adaptation strategy that secures sustainable

domestic water supplies, while also addressing the needs of agriculture, industry, and ecosystem health, in the face of increasing population and economic activity.

An integrated water resource management (IWRM) framework, incorporating stakeholder engagement and participatory decision-making, is essential for sustainable water management in Davao City. This framework should be based on scientific data and incorporate local knowledge and values. Multi-stakeholder platforms, involving government agencies, water utilities, NGOs, and community groups, should be established to facilitate the development and implementation of water management plans. Results from hydrological modeling and water quality assessments should be communicated effectively to the public to raise awareness about water-related risks and promote water conservation

When facing a projected recharge decline, particularly in a context like Davao City, a combination of adaptive strategies is essential. Managed Aquifer Recharge (MAR) and afforestation are two key approaches. Another suggestion is the source water diversification, targeted reforestation in recharge areas, riparian zone restoration, among others. By implementing these adaptive strategies, Davao City can enhance its resilience to projected recharge decline and ensure long-term water security.

Funding: The researcher is grateful to the Commission on Higher Education (CHED) for the scholarship and dissertation financial assistance. The researcher is indebted to the International Development and Research Center (IDRC) and its partner institution, University of Nairobi for the huge opportunity, providing financial assistance to the conduct of the whole study.

Acknowledgments:

The successful completion of this research was significantly aided by the insightful guidance of the advisory committee, comprising Dr. Juan M. Pulhin, Dr. Rex Cruz, Dr. Rodel D. Lasco, and Dr. Carmelita M. Rebanocos. We also deeply appreciate the expert tutoring provided by Dr. Edwin Combalicer and Francis John Federoga in utilizing the BROOK90 hydrological model and SDSM. Finally, we extend our sincere thanks to the Davao City Water District and the PAG ASA Meteorological station at Bago Oshiro, Davao City, for their generous provision of crucial data.

Conflicts of Interest: The author declares no conflicts of interest. Further, the funders had no role in the design of the study; in the collection, analysis, or interpretation of data; in the writing of the manuscript; or in the decision to publish the results.

REFERENCES

Bamala, A., Uddin, M.G. and Olbert, A.I., 2024. Harnessing machine learning for assessing climate change influences on groundwater resources: A comprehensive review. *Heliyon*, 10(17), p.e37073.¹ Available from: <https://doi.org/10.1016/j.heliyon.2024.e37073>

Bates, B., Kundzewicz, Z.W., Wu, S., & Palutikof, J.P., 2008. *Climate Change and Water*. Technical Paper VI of the Intergovernmental Panel on Climate Change. Intergovernmental Panel on Climate Change Secretariat, Geneva, 210 pp.

Branzuela, N.E., Faderogao, F.J.F., & Pulhin, J.M., 2015. Downscaled Projected Climate Scenario of Talomo-Lipadas Watershed, Davao City, Philippines. *Journal of Earth Science & Climate Change*, 6(268). <https://doi.org/10.4172/2157-7617.1000268>

Benz, S.A., Irvine, D.J., Rau, G.C., Bayer, P., Menberg, K., Blum, P., Jamieson, R.C., Griebler, C. and Kurylyk, B.L., 2024. Global groundwater warming due to climate change. *Nature Geoscience*, 17(6), pp.545-551.¹ Available from: <https://doi.org/10.1038/s41561-024-01453-x>

Combalicer, E. A., Cruz, R.V.O., Lee, S., & Im, S., 2010. Assessing Climate Change Impacts on Water Balance in the Mount Makiling Forest, Philippines. *Journal of Earth Science*, 119(3), 265-283.

Hearne, D., 2011. *Customized IWRM Guidelines for Davao City and Region*. First Edition. HELP Davao Network.

Dao, P.U., Heuzard, A.G., Le, T.X.H., Zhao, J., Yin, R., Shang, C. and Fan, C., 2024.¹ The impacts of climate change on groundwater quality: A review. *Science of The Total Environment*, 912, p.169241.¹ Available from: <https://doi.org/10.1016/j.scitotenv.2023.169241>

Davamani, V., John, J.E., Poornachandra, C., Gopalakrishnan, B., Arulmani, S., Parameswari, E., Santhosh, A., Srinivasulu, A., Lal, A. and Naidu, R., 2024. A Critical Review of Climate Change Impacts on Groundwater Resources: A Focus on the Current Status, Future Possibilities, and Role of Simulation Models.¹ *Atmosphere*, 15(1), p.122. Available from: <https://doi.org/10.3390/atmos15010122>

Dettinger, M.D., & Earman, S., 2007. Western groundwater and climate change—pivotal to supply sustainability or vulnerable in its own right? *Ground Water*, 45(1), 4-5. <https://doi.org/10.1111/j.1745-6520.2006.00892.x>

Famiglietti, J.S., 2014. The global groundwater crisis. *Nature Climate Change*, 4(11), pp.945-948. Available from: <https://doi.org/10.1038/nclimate2422>

Fasullo, J.T., Trenberth, K.E., Walsh, J.E. and Washington, W.M., 2015. Global warming of the climate system. *Reviews of Geophysics*, 53(3), pp.450-483. Available from: <https://doi.org/10.1002/2014RG000485>

Federer, C.A., Vörösmarty, C., & Fekete, B., 2003. Sensitivity of annual evaporation to soil and root properties in two models of contrasting complexity. *Journal of Hydrometeorology*, 4(6), 1276-1290. [https://doi.org/10.1175/1525-1036\(2003\)004<1276:SOAAET>2.0.CO;2](https://doi.org/10.1175/1525-1036(2003)004<1276:SOAAET>2.0.CO;2)

Ficklin, D.L., Letsinger, S.L., Stewart, I.T. and Maurer, E.P., 2018. Projected climate change impacts on streamflow in the western United States. *Journal of Hydrology*, 564, pp.976-993. Available from: <https://doi.org/10.1016/j.jhydrol.2018.07.050>

Flatto, G.M., & Boer, G.J., 2001. Warming asymmetry in climate change simulations. *Geophysical Research Letters*, 28(10), 195-198. <https://doi.org/10.1029/2000GL012217>

Green, T.R., Taniguchi, M., Kooi, H., Gurdak, J.J., Allen, D.M., Hiscock, K.M., Treidel, H. And Aureli, A., 2007. Beneath the surface of global change: Impacts of climate change on groundwater. *Journal of Hydrology*, 405(3-4), pp.532-560.

Green, T.R., Taniguchi, M., Kooi, H., Gurdak, J.J., Allen, D.M., Hiscock, K.M., ... & Aureli, A., 2011. Beneath the surface of global change: Impacts of climate change on groundwater. *Journal of Hydrology*, 405(3-4), 532-560. <https://doi.org/10.1016/j.jhydrol.2011.05.002>

Hatfield, J.L. & Prueger, J.H., 2015. 'Temperature extremes: Effect on plant growth and development', *Weather and Climate Extremes*, vol. 10, pp. 4-10. Available at: <https://doi.org/10.1016/j.wace.2015.08.00>

IPCC., 2000. *IPCC Special Report Emissions Scenarios. Summary for Policy Makers*. IPCC. <https://www.ipcc.ch/site/assets/uploads/2018/03/sres-en.pdf>

Intergovernmental Panel on Climate Change (IPCC), 2021. *Climate change 2021: The physical science basis*. Contribution of Working Group I to the Sixth Assessment Report of the Intergovernmental Panel on Climate Change. Cambridge University Press. <https://doi.org/10.1017/9781009157896>

Kruger, A., Ulbrich, U., & Speth, P., 2001. Groundwater recharge in Northrhine-Westfalia predicted by a statistical model for greenhouse gas scenarios. *Physics and Chemistry of the Earth, Part B: Hydrology, Oceans and Atmosphere*, 26(11-12), 853-861. [https://doi.org/10.1016/S1474-7065\(01\)00085-5](https://doi.org/10.1016/S1474-7065(01)00085-5)

Kundzewicz, Z.W., Mata, L.J., Arnell, N.W., Doll, P., Kabat, P., Jimenez, B., Miller, K.A., Oki, T., Sen, Z., Shiklomanov, I.A., 2007. Freshwater resources and their management. In: Parry, M.L., Canziani, O.F., Palutikof, J.P., van der Linden, P.J., Hanson, C.E. (Eds.), *Climate Change 2007: Impacts, Adaptation and Vulnerability*. Cambridge University Press, Cambridge, pp. 173–210

Kiniry, J.R., 2012. *Input documentation for SWAT2012*. USDA Agricultural Research Service and Texas A&M AgriLife Research.

Morris, C.E., Simmonds, I. and Plummer, N., 2017. Quantifying the impact of observed land cover change on Australian climate. *Geophysical Research Letters*, 44(14), pp.7461-7468. Available from: <https://doi.org/10.1002/2017GL074242>

Nyeko-Ogiramoi, P., Ngirane-Katashaya, G., Willems, P., & Ntegeka, V., 2010. Evaluation and inter-comparison of Global Climate Models' performance over Katonga and Ruizi catchments in Lake Victoria basin. *Physics and Chemistry of the Earth, Parts A/B/C*, 35(15-18), 618-633.

Paul, M. J., 2006. Impact of land-use patterns on distributed groundwater recharge and discharge. *Chinese Geographical Science*, 16(3), 229-235. DOI: 10.1007/s11769-006-0229-5

Parmesan, C. & Yohe, G. (2003) A globally coherent fingerprint of climate change impacts across natural systems. *Nature*, 421(6918), pp. 37–42. doi: 10.1038/nature01070.

Philippines Environment Monitor, 2003. *Philippines Environment Monitor 2003*. Country Office, Manila: World Bank. Available at: www.worldbank.org.ph [Accessed 9 Apr. 2025]

Rosenzweig, Cynthia; Iglesias, Ana; Yang, X. B.; Epstein, Paul R.; and Chivian, Eric, 2001. "Climate change and extreme weather events - Implications for food production, plant diseases, and pests". NASA Publications. 24. <https://digitalcommons.unl.edu/nasapub/24>

Satterlund, D. R. 1972. *Wildland watershed management*. N. Y.: The Ronald Press Co.

Tubiello, F.N. et al. (2007) Effects of climate change on agricultural production. *European Journal of Agronomy*, 26(4), pp. 449–462. doi: 10.1016/j.agrformet.2006.09.009.

Vacarro, J. J., 1992. Sensitivity of groundwater recharge estimates to climate variability and change, Columbia Plateau, Washington, J. Geophys. Res. 97 (D3), 2821-2833.

Vorobevskii, I.I., 2020. R-Based Framework for BROOK90 Hydrological Model: Implementation and Application for Forested Catchment. *Environmental Modelling & Software*, 132, p.104800. Available from: <https://doi.org/10.1016/j.envsoft.2020.104800>

Wilby, R.L., Dawson, C.W. and Barrow, E.M., 2002. SDSM—a decision support tool for the assessment of regional climate change impacts. *Environmental Modelling & Software*, 17(2), pp. 147-159.

Wu, W., Lo, M., Wada, Y., Famiglietti, J.S., Reager, J.T., Yeh, P.J., Ducharne, A. and Yang, Z., 2020. Divergent effects of climate change on future groundwater availability in key mid-latitude aquifers. *Nature Communications*, ¹ 11(1), pp.1-9. Available from: <https://doi.org/10.1038/s41467-020-17581-y>

Zektser, I.S. and Loaiciga, H.A., 1993. Groundwater fluxes in the global hydrologic cycle, past, present, and future. *Journal of Hydrology*, 144(1-4), pp. 405-427.